Journal Pre-proofs

Pyrolysis and in-line catalytic decomposition of excavated landfill waste to produce carbon nanotubes and hydrogen over Fe- and Ni-based catalysts – Investigation of the catalyst type and process temperature

Katarzyna Jagodzińska, Pär Göran Jönsson, Weihong Yang

PII: S1385-8947(22)02303-8
DOI: https://doi.org/10.1016/j.cej.2022.136808
Reference: CEJ 136808

To appear in: *Chemical Engineering Journal*

Received Date: 27 February 2022
Revised Date: 30 April 2022
Accepted Date: 2 May 2022

Please cite this article as: K. Jagodzińska, P. Göran Jönsson, W. Yang, Pyrolysis and in-line catalytic decomposition of excavated landfill waste to produce carbon nanotubes and hydrogen over Fe- and Ni-based catalysts – Investigation of the catalyst type and process temperature, *Chemical Engineering Journal* (2022), doi: https://doi.org/10.1016/j.cej.2022.136808

Pyrolysis and in-line catalytic decomposition of excavated landfill waste to produce carbon nanotubes and hydrogen over Fe- and Ni-based catalysts – Investigation of the catalyst type and process temperature

Katarzyna Jagodzińska[1,*], Pär Göran Jönsson[1], Weihong Yang[1]

[1] KTH Royal Institute of Technology, Department of Material Sciences and Engineering, Brinellvägen 23, Stockholm, Sweden

[*] Corresponding author. E-mail address: kjag@kth.se (K. Jagodzińska).

Abstract. Undeniably, non-sanitary landfills existing worldwide pose considerable environmental risks related to air, water and soil pollution. Despite that, the landfill mining concept does not spread swiftly around the world. To prevent its fading into oblivion, it is necessary to transform the perception of landfills as waste to seeing them as stocks of valuable materials. Guided by this idea, this novel study investigates the possibility of producing carbon nanotubes (CNTs) and hydrogen-rich gas, materials crucial for our transition towards a more sustainable future, from excavated waste as these. To the best of our knowledge, this is the first study on catalytic pyrolysis of excavated waste. For this purpose, excavated waste was subjected to pyrolysis followed by in-line catalytic decomposition of the produced pyrovapours. The impact of the catalyst type and catalyst bed temperature on the process performance was analysed. Six types of monometallic and bimetallic Ni- and Fe- based catalysts, synthesised using two methods (the sol-gel and the impregnation method), were considered. Three catalyst bed temperatures were taken into account, namely 700°C, 800°C, and 900°C. The results showed that the bimetallic catalyst prepared by using the sol-gel method (FeNi/Al_Sg) outperformed the other analysed catalysts, yielding 9 mmol/g_{sample_daf} of H_2 and 76 mg/g_{sample_daf} of CNTs at 800°C. The product yields and quality were comparable to those reported in the open literature for homogeneous plastic waste pyrolysis. Eventually, the future research directions were discussed.

Keywords. Enhanced landfill mining, waste management, circular economy, sol-gel, impregnation

1. Introduction

Undoubtedly, a circular economy concept spreads over all economic and social activities around the world. One of the concept's pillars is recovering anthropogenic resources, including the so-called stocks (i.e., old landfills) [1,2]. Their recovery is referred to as landfill mining or Enhanced Landfill Mining (ELFM) when it encompasses recovering material and energy from excavated waste and simultaneously fulfilling rigorous ecological and social criteria [2].

The ELFM is an emerging concept, and, consequently, it suffers from deficiencies in a systematic knowledge of it as a whole and its economic performance [3]. This hinders its spreading around the world. One of the aspects requiring more research is the energy recovery from excavated waste. Hitherto, incineration has been considered to be the most suitable way of excavated waste valorisation as it is a better-established technology than gasification or pyrolysis [4–7]. However, waste incineration is not covered by a greater objective of the circular economy concept. Therefore, alternatively, plasma gasification was identified as a viable technology for material and energy recovery from excavated waste [8,9]. Accordingly, several studies have been performed on excavated waste gasification [10–13]. This process, however, still faces some unknowns related to the quality or marketability of the obtained products. Therefore, more research on the topic is required [10,11,14,15].

Along with a need for more research on excavated waste gasification, the need for more research on other waste-to-energy technologies was raised [16,17]. As one of the technologies complementary to gasification, pyrolysis offers a method of excavated waste valorisation [18–20]. For this reason, a lab-scale study on the pyrolysis of refuse-derived fuel (RDF) formed from excavated waste was performed [21]. Due to a complex feedstock composition, the obtained condensables were not of commercial interest, but they showed the potential for being upgraded to higher-quality products [21]. Ergo, this study aims at investigating the possibility of their upgrading.

The analysed RDF formed from excavated waste is characterised by a high content of plastics – approx. 60wt% of the non-inert part of the feedstock, from which over 50wt% is PE. The pyrolysis process followed by in-line catalytic decomposition (without using steam) was chosen in this study as, according to

Yao et al. [22], for olefin types of plastics (e.g., PE), thermal decomposition reactions are favoured over steam reforming reactions to produce higher hydrogen yields.

Hitherto, numerous studies on pyrolysis and in-line catalytic decomposition of mono-mixtures of plastics [23–25] or the so-called 'real-world' waste plastics [26–29] were performed. Most of them focused on the production of hydrogen along with carbon nanotubes (CNTs), as both have a vast number of industrial applications [30–32]. Hydrogen is considered a clean fuel and is firmly rooted in future energy scenarios [33]. Presently, however, it is predominantly produced from fossil fuels, and due to their phasing out, adopting alternative H_2 sources is of crucial importance [34]. Carbon nanotubes (CNTs) have attracted attention due to their characteristics of, among others, high electrical conductivity and tensile strength over 100 times greater than that of stainless steel [35–38]. For that reason, they are used in numerous industrial applications (e.g., as electrically conductive fillers in composite plastic materials, as supercapacitor electrodes and adsorbents for environmental remediation, in photoelectrodes, or even in biomedicine) [30–32,38–40]. Up to now, CNTs produced from waste plastics have been positively assessed in a few applications, for instance, as strengthening reinforcement in the fabrication of composite materials or for herbicide removal from wastewater [39,41].

In the light of the foregoing, pyrolysis followed by in-line catalytic decomposition poses a considerable potential for answering future demands of H_2 and CNTs. For the purpose of their production, various catalysts have been used, but Fe- and Ni-based catalysts are the most common due to their favourable ratio between catalytic activity and price [42,43]. Similarly, various catalyst supports were used, but γ-Al_2O_3 is most common due to its chemical and psychical stability, high mechanical resistance, and strong interactions with transition metals allowing their better dispersion among the support [26,44]. For these reasons, Fe- and Ni-based catalysts on γ-Al_2O_3 support were investigated within the study.

Besides catalyst composition, a catalyst synthesis method is another element to consider [45]. In previous studies, catalysts were synthesised using co-precipitation, impregnation, and sol-gel methods [26,46,47]. Yao et al. [22] investigated the influence of different catalyst synthesis methods on the hydrogen yield. The catalyst prepared using the sol-gel method was characterised by a higher surface area and more uniform metal dispersion than catalysts prepared using the impregnation or co-precipitation methods. Consequently, the sol-

gel catalyst generated a higher H_2 yield, followed by the impregnation catalyst. Therefore, these two synthesis methods were chosen for the current study.

Another crucial parameter in catalytic decomposition is catalyst bed temperature. Several studies have been performed regarding pyrolysis with in-line catalytic decomposition using temperatures in the range of 550-900°C. However, no consensus on the influence of catalytic bed temperature on the CNTs quality was reached. For instance, Acomb et al. [48] and Yao et al. [26] observed intensification of the filamentous carbon formation with temperature increase from 700°C to 900°C; however, the quality of these deposits decreased at 900°C in comparison to that at 800°C. On the contrary, Zhang and Williams [49], Liu et al. [50], and Mishra et al. [51] observed not only an increase in the amount of filamentous carbon produced but also in its quality (graphitisation) with temperature increase. This discrepancy might be related to differences in feedstocks (e.g., waste tires and different types of plastics), reactors, or catalysts used. Therefore, in this study, the analysis was expanded to include different catalyst bed temperatures (in the range of 700°C-900°C).

Several types of two-stage reactors have been used for the pyrolysis process with in-line catalytic decomposition. Batch fixed bed-fixed bed reactors were used extensively in previous research [52–54] due to their relative simplicity of construction, operation, and maintenance. For these reasons, such a configuration was used in this study as it is a preliminary study on the matter, which will be the base for further research. On the other hand, Namioka et al. [55] and Wu and Williams [56] took a step further and used a two-stage fixed bed reactor with a continuous feeding system for pyrolysis and in-line steam reforming of waste plastics. This was done to bring the process closer to the continuous commercial systems and deeper analyse the impact of operating parameters on the quality of process products. Other researchers used, for instance, a conical spouted-bed reactor coupled with fixed-bed [57] or fluidised-bed reactors [58–60]. Using a conical spouted-bed reactor minimises bed agglomeration problems due to plastics fusing in continuous systems [57], whereas the fluidised-bed reactors were used to avoid bed blockage and gas flow circulation issues caused by carbon deposition [59]. Last but not least, the set-ups consisting of two fluidised-bed stages were used to enable the production of larger CNTs amounts [39].

To sum up, an investigation of pyrolysis and in-line catalytic decomposition of excavated waste was performed. To the best of our knowledge, this is the first study on catalytic pyrolysis of excavated waste. The

process was performed for six Fe- and Ni-based catalysts using pyrolysis and catalytic bed temperatures of 600°C and 800°C, respectively. Additionally, the influence of catalytic bed temperature on the catalyst performance was investigated – in this case, two additional catalyst bed temperatures (700°C and 900°C) were taken into account. The process products were extensively characterised, and their quality was assessed and discussed. The feedstock used within the study was RDF made of excavated waste from an existing Belgian landfill site.

2. Material and methods

2.1. Feedstock properties

The refuse-derived fuel (RDF) used within the study was extensively described in the work by Jagodzińska et al. [21]; hence only an abridged description is presented herein.

The RDF was formed from waste excavated at the old part of the Mont-Saint-Guibert landfill in Belgium [61]. A total of 130 m^3 of the buried waste (construction and demolition waste, municipal solid waste, and non-hazardous industrial waste), disposed of at the landfill between 1958 and 1985, was excavated. Subsequently, the material was ballistically sorted into three fractions (light, heavy and fine fractions). However, only a light fraction (particle size of 90-200 mm) was selected for this study due to its relatively high heating value and low level of impurities. The chosen fraction was ground to particle sizes below 3 mm prior to the tests to improve its homogeneity and to enable the performance of lab-scale tests with a certain repeatability.

The feedstock's composition is shown in Table 1 [21,61]. It is characterised by a high ash content related predominantly to a high content of the so-called *fine* fraction (soil-like material) and impurities adhered to the surface of other fractions, e.g. plastic particles. The so-called *2D plastic* fraction is primarily made of thin PE fragments, whereas the *3D plastic* fraction is a mixture of PVC, PE, PP and PS [62]. The so-called *rest* fraction (the remaining unclassified fraction) consists mainly of foam, rubber, and lignocellulosic material [62]. The feedstock is characterised by a high Cl content, predominantly related to PVC presence among the *3D plastic*

fraction, whereas sulphur content can be linked to the presence of sulphur cross-linked rubber particles among the *rest* fraction [62].

Table 1 Composition of the feedstock in a dry state [21,61]

Fraction	Content, wt%	Compound/element	Content, wt%
Wood	0.7	ash	46.48 ± 4.65
Paper	3.5	moisture	1.5 ± 0.15
Textile	8.4	C	40.5 ± 2.025
2D plastic	37.5	H	6.1 ± 0.61
3D plastic	4.8	N	1.1 ± 0.11
Ferrous metals	1.7	S	0.234 ± 0.023
Non-ferrous metals	0.2	Cl	1.203 ± 0.301
Inert	1.5	O (calculated)	4.3
Rest	10.5		
Fines (particles < 20 mm)	31.2		

2.2. Catalysts preparation

Six types of Fe- and Ni-based catalysts were used within the study – four monometallic and two bimetallic. For the bimetallic catalysts, the molar ratio between Fe and Ni was 3:1, following the study of Yao et al. [27], in which such a ratio resulted in the highest yield of hydrogen and CNTs.

The catalysts were prepared using impregnation and sol-gel methods with an initial metal loading of 10wt%, following the procedure described by Yao et al. [22]. For the impregnation method, the metal nitrates (Sigma Aldrich, 99.999% for $Ni(NO_3)_2{\cdot}6H_2O$ and 98%+ for $Fe(NO_3)_3{\cdot}9H_2O$) were dissolved in absolute ethanol (Fisher Chemical, 99%+), and subsequently, γ-Al_2O_3 (Alfa Aesar™, 99.9%) was added. The mixture was continuously stirred until it formed a slurry. Prior to calcination in air at 750°C for 3 h (holding time), the mixture was dried overnight at 50°C to remove the excessive ethanol. For the sol-gel method, initially, aluminium tri-sec-butoxide (ATB, Sigma Aldrich, 97%) was dissolved in absolute ethanol (Fisher Chemical, 99%+), and the mixture was

stirred at 50°C for 2.5 h until a homogeneous slurry was formed. Simultaneously, metal nitrates were dissolved in deionised water. After stirring the ATB-ethanol mixture, the metal nitrates solution was slowly added to the mixture. The formed mixture was then stirred at 75°C for 30 min. 1M nitric acid was used as a pH adjusting agent until the mixture reached a pH value of 4.8. The obtained catalyst was dried and, afterwards, calcinated in air at 550°C for 3 h (holding time). After the calcination, the catalysts were crushed and sieved to the particle size of 75-200 µm. No reduction of the catalysts was performed before the tests as vapours generated during the pyrolysis reduce the metal oxides in-situ [26].

The catalysts prepared using the impregnation method are further referred to as Ni/Al_Im, Fe/Al_Im and FeNi/Al_Im, and the catalysts prepared using the sol-gel method were marked as Ni/Al_Sg, Fe/Al_Sg, and FeNi/Al_Sg.

2.3. Pyrolysis tests

The tests were performed in a fixed bed reactor shown in Fig. 1. The test rig comprises two electrically heated stainless steel reactors (inner diameter of 24 mm), a condensing section with a cooling jacket and a set of impingers immersed in a cooling bath, and an aerosol trap. The pyrolysis temperature is controlled by the thermocouple immersed in the sample ceramic basket, whereas the catalytic bed temperature is regulated by the thermocouple below the catalytic bed. The first stage of the reactor is also equipped with a cooling zone, and the cooling agent (isopropanol/water mixture at -15°C) circulates between the cooling jacket, cooling bath, and cooling zone.

The test procedure was as follows: 2 g of feedstock sample (dried overnight at 80°C) was placed in the first stage of the reactor, whereas 1 g of catalyst (or sand in the case of reference tests without any catalyst) was placed in the second stage of the reactor in the stainless-steel basket. The feedstock/catalyst ratio of 2 was chosen following the findings of Saad and Williams [63]. From the beginning of the reactor heating, it was being flushed with nitrogen (250 ml/min) to ensure that an inert atmosphere of the reaction was obtained. The pyrolysis temperature was set at 600°C to minimise the solid residue yield [21], whereas the catalytic bed temperature was set at 800°C as this temperature was found to be optimal in previous studies [48,63,64]. In the part of the study focused on investigating the influence of catalytic bed temperature on the catalyst performance, the catalytic bed temperature was set at 700°C and 900°C. When the reactor reached the desired temperature,

the sample was promptly introduced to the first stage and kept there for 30 min. The produced volatiles flew through the second stage of the reactor with the catalyst bed and, afterwards, through the condensing section, where condensables were collected. The non-condensable volatiles (non-condensables) flew further to a drum-type gas meter (TG1 type, Ritter, Germany), and, subsequently, they were collected in a Tedlar™ gas sample bag to enable a determination of their total composition using the Micro GC (490 Micro GC System QUAD, Agilent). The sample basket, the catalyst basket, the elements of the condensing sections (cooling jacket, impingers), and an aerosol trap were weighed before and immediately after the experiment to determine the product yields. Eventually, the closure of the mass balance was done by calculating the non-condensables yield from their known composition and flow. Additionally, H_2 yield and H_2 conversion rate were given separately in the manuscript. The H_2 yield was calculated using the known (measured) volumetric content of hydrogen in gas and the total gas volume. The H_2 conversion rate was calculated using the known volumetric content of hydrogen in gas (converted to mass) and the known mass of theoretical maximum H_2 yield (calculated from the measured H_2 content in the sample and the sample mass). Random order of tests was introduced to avoid consecutive run errors, and the tests were repeated at least 2 times to ensure a good repeatability of the results.

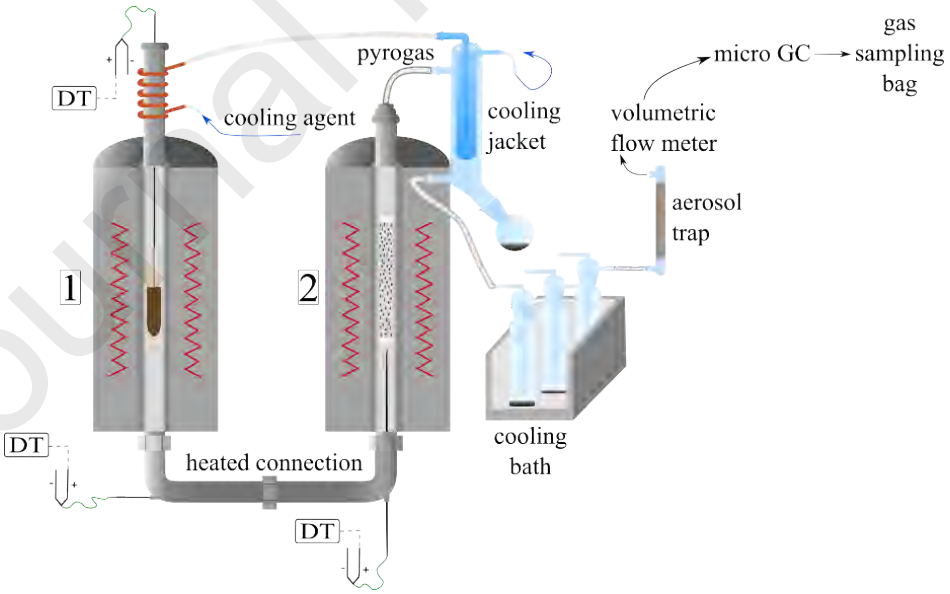

Fig. 1 A general scheme of the test rig (C - cooling zone; DT - digital thermometer; 1,2 – first and second stage of the reactor)

2.4. Pyrolysis products characterisation

The condensables were collected using a DCM/methanol solution (volume ratio of 1/2). Their water content, analysed by Karl Fischer titration (T5 titrator, Meter Toledo), did not exceed 2.5wt%. Their composition was analysed using GC/MS (Agilent 7890A/Agilent 5975C) with a DB-1701 column (30 m × 0.25 mm × 0.25 μm, Agilent). The MS scanning range was m/z 45-300, with a frequency of 2.83 scans/sec. The MS source and quadrupole temperatures were 230°C and 150°C, respectively. Samples were introduced to the GC injector at 280°C (splitless) with helium as a carrier gas (1 ml/min). The temperature profile was as follows: holding at 35°C for 5 min, heating with 3°C /min to 280°C, and holding for 3 min with five isothermal 3-minute steps in between at 137°C, 152°C, 236°C, 260°C, 263°C. In order to enable a comparison between the results of the repetitions (condensables obtained within the same case for one catalyst or no catalyst), the weight-normalisation of the GC/MS results was done. The weight-normalisation was done by dividing the peak areas by the weight of condensables from each experiment. After that, the repetitions' results were combined, and the identification of compounds was done manually using the NIST-11 library with a minimum match factor of 85%. Additionally, the identification of chosen compounds (2-methylnaphthalene, acenaphthene, anthracene, benzo[a]pyrene, benzo[e]pyrene, biphenylene, fluoroanthene, fluorene, naphthalene, perylene, phenanthrene, pyrene, triphenylene) was verified using the reference standards of a chromatographic grade (Sigma Aldrich, Sweden). The total weight-normalised area% of those compounds was above 84% of the total weight-normalised area% of all detected compounds.

The collected non-condensables were analysed using the Micro GC (490 Micro GC System QUAD, Agilent), equipped with Molsieve 5Å, PoraPLOT U, Al_2O_3/KCl, and CP-Sil 5CB columns. The Micro GC was calibrated for N_2, O_2, H_2, CH_4, CO, CO_2, H_2S, and C_2-C_4 hydrocarbons.

The proximate composition of the solid residue was analysed according to the EN-ISO 18122:2015 (ash content) and EN 15414-3:2011 (moisture content) standards [65,66].

2.5. Catalyst characterisation

To characterise the fresh catalysts, multiple techniques were used. First of them was X-ray diffraction (XRD; D8 Discover, Bruker) analysis performed using a Cu Kα radiation (λ = 0.15418 nm) with an X-ray generator

voltage of 40 kV and the current of 40 mA, using a scanning step of 0.0249°/s in the 2θ range of 10-89°. Peaks were identified using the DIFFRAC.EVA software package. The second technique was a temperature-programmed reduction (TPR; AutoChem 2910, Micromeritics) performed in a hydrogen atmosphere (5vol% of H_2 balanced by Ar). Around 0.2 g of the sample was preheated to 300°C and held for 1 h, and, subsequently, cooled down and heated up again to 900°C using a heating rate of 10°C/min. Additionally, an external lab (Department of Materials and Environmental Chemistry, Stockholm University) determined the porous properties of the catalysts. For this purpose, the N_2 adsorption-desorption measurement was performed using a Micromeritics ASAP 2020 instrument, and the catalyst's surface area was calculated using Brunauer-Emmett-Teller (BET) method. The total pore volume was determined at a relative pressure p/p_0 of 0.99, and the pore distribution was obtained from the desorption isotherms using the Barrett-Joyner-Halenda (BJH) method. The BJH average pore width was calculated from the BJH average adsorption and desorption pore widths. The samples were degassed at 250°C for 12 h prior to the measurement. The morphology and metal dispersion over the catalyst were examined using a scanning electron microscope (SEM; S3700N, Hitachi).

The yield of coke deposition on spent catalysts was determined as C content measured according to the EN 15407:201 standard (Vario EL cube CHNS elemental analyser, Elementar) [67]. The character of coke deposition was examined using temperature-programmed oxidation (TPO; STA 449 F1 Jupiter, NETZSCH) in approx. 5vol% of O_2 balanced by N_2. 0.250-0.35 g of the spent catalyst was heated up at 10°C/min to 120°C, heated further up at 5°C/min to 850°C, and held for 2 min. As amorphous carbon is more reactive than filamentous deposition [43], it yields a TPO peak at lower temperatures – below 500°C [57,58,68]. Therefore, the mass loss at temperatures below 500°C is associated with amorphous coke mass, whereas the mass loss at higher temperatures is attributed to filamentous carbon deposits. The graphitic nature of the coke deposits was examined by an external lab (Department of Materials and Environmental Chemistry, Stockholm University) using a Raman spectroscopy (LabRAM HR 800, Horiba) with a green laser (wavelength of 532 nm) and a Raman shift of 100-3000 cm^{-1}. Additionally, the chosen spent catalyst (with the highest quality of carbon deposits) was examined using a field emission scanning electron microscope (FE-SEM; HI-9044-0005, Hitachi).

3. Results and discussion

3.1. Fresh catalysts characterisation

The BET surface areas and pore size properties of the fresh catalysts are shown in Table 2. The physisorption isotherms for the catalysts are shown in Fig. A1 in the Supplementary material. Fresh catalysts were also characterised using XRD (Fig. 2) and TPR (Fig. 3). Additionally, the results of the SEM analysis are shown in Fig. A2-3 in the Supplementary material.

The catalysts prepared using the sol-gel method are characterised by having significantly higher BET surface areas than those prepared using the impregnation method (Table 2), which is in line with the findings of Yao et al. [22,23]. Similarly, their pore volumes and BJH average pore sizes are higher. The exceptions are Ni-based catalysts characterised by similar BJH average pore widths. However, the Ni/Al_Sg catalyst has more than two times higher pore volume than the Ni/Al_Im catalyst, indicating that it has a more porous structure. According to the IUPAC classification, all of the obtained physisorption isotherms are type IV (Fig. A1 in the Supplementary material), which, along with the average pore width in the range of 8-11 nm, means that they can be categorised as mesoporous materials [69]. Furthermore, the sol-gel catalysts show a more 'fluffy' structure than the impregnation catalysts in the SEM analysis (Fig. A2-3 in the Supplementary material), additionally indicating their higher surface area [23,70]. The SEM analysis also shows the uniform dispersion of metals among the catalysts with a slight Fe agglomeration in the bimetallic catalysts.

Table 2 The porosity analysis results for the fresh catalysts

Catalyst	**BET surface area, m^2/g**	**Pore volume, cm^3/g**	**BJH average pore width, nm**
Ni/Al_Im	81.90	0.20	8.24
Fe/Al_Im	81.18	0.21	7.86
FeNi/Al_Im	82.97	0.21	8.08
Ni/Al_Sg	240.41	0.49	8.25
Fe/Al_Sg	224.43	0.71	11.12
FeNi/Al_Sg	239.60	0.65	9.79

The XRD results for the sol-gel catalyst show their more amorphous nature than that of the catalysts prepared using the impregnation method, which yielded intense and sharp peaks indicating their more crystalline nature (Fig. 2) [26,71]. The XRD profiles for the catalysts agree with the findings of the previous studies [26,43,72]. Fe_2O_3 was identified extensively in the Fe/Al_Im catalyst, as reported in Acomb et al. [43]. Besides Al_2O_3, NiO and $NiAl_2O_4$ were detected in the case of Ni/Al_Im, as reported in Saad et al. [72]. Moreover, the presence of spinels ($FeAlO_3$ and $NiAl_2O_4$) in all analysed catalysts indicates the enhanced interaction between metal and catalyst support [26]. In the case of bimetallic catalysts (FeNi/Al_Im and FeNi/Al_Sg), peaks related to NiO or $NiAl_2O_4$ are not well pronounced due to relatively low Ni contents (Fe:Ni ratio of 1:3). Following Dong et al. [68], the lower the Ni content, the stronger metal-support interactions, which lead to the formation of $NiAl_2O_4$ spinels. In addition, the presence of Ni and Fe was detected in sol-gel catalysts, which is in line with the findings of Yao et al. [22].

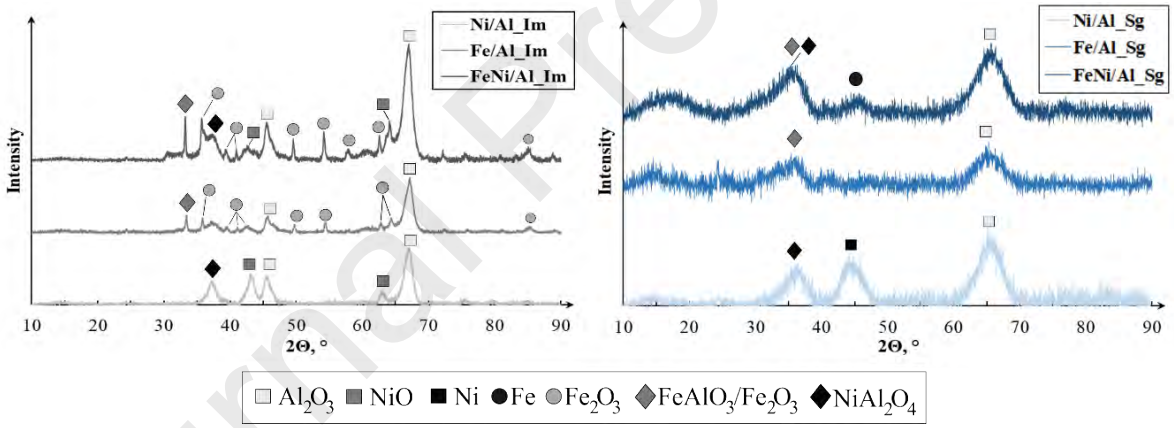

Fig. 2 XRD analysis for the fresh catalysts

The obtained TPR profiles for the impregnation and sol-gel catalysts differ significantly (Fig. 3). The Ni/Al_Im catalyst shows two main peaks at around 580°C and 800°C, which may be associated with the reduction of NiO and $NiAl_2O_4$, respectively [59,68]. Similarly, the peak at 700-800°C for the Ni/Al_Sg catalyst is associated with $NiAl_2O_4$. Nevertheless, only a slight peak at around 430°C was detected for the Ni/Al_Sg, which might indicate the presence of a surface or bulk NiO weakly bonded to the base material [41]. NiO was, however, not detected in the XRD analysis for the Ni/Al_Sg catalyst, which, as mentioned before, might be related to its small amount in the catalyst [68]. On the contrary, Fe/Al_Im and Fe/Al_Sg catalysts show a main

peak at 470°C and 500°C, respectively. Following Park et al. [73], this peak is related to the conversion of Fe_2O_3 to Fe_3O_4, and further overlapping and asymmetric peaks are related to the reduction of Fe_3O_4 to FeO and, eventually, to Fe. Additionally, a pronounced peak at a temperature higher than 850°C for Fe/Al_Sg indicates the presence of barely reducible Fe-Al spinel structures.

A merged series of peaks for FeNi/Al_Sg at 600-900°C (Fig. 3) indicate the presence of different mixed Fe oxides and Fe-Al spinels [74,75]. A slight peak shift to lower temperatures can be observed for the bimetallic catalysts compared to the Fe-based catalysts, as they occur at 425°C and 450°C for FeNi/Al_Im and FeNi/Al_Sg catalysts, respectively. The bimetallic interactions occurring in the Fe-Ni catalysts were also observed by Winter et al. [76] and Huang et al. [77]. It is most likely caused by the presence of Ni promoting the reduction of Fe species [23,78]. This improved reducibility might indicate a higher activity of bimetallic catalysts over monometallic catalysts [23].

In general, all analysed catalysts showed intermediate metal-support interactions (Fig. 3) except for Fe/Al_Sg, which mainly yielded one peak at a temperature below 600°C and no pronounced peaks at the higher temperature, which suggest weaker metal-support interactions [43].

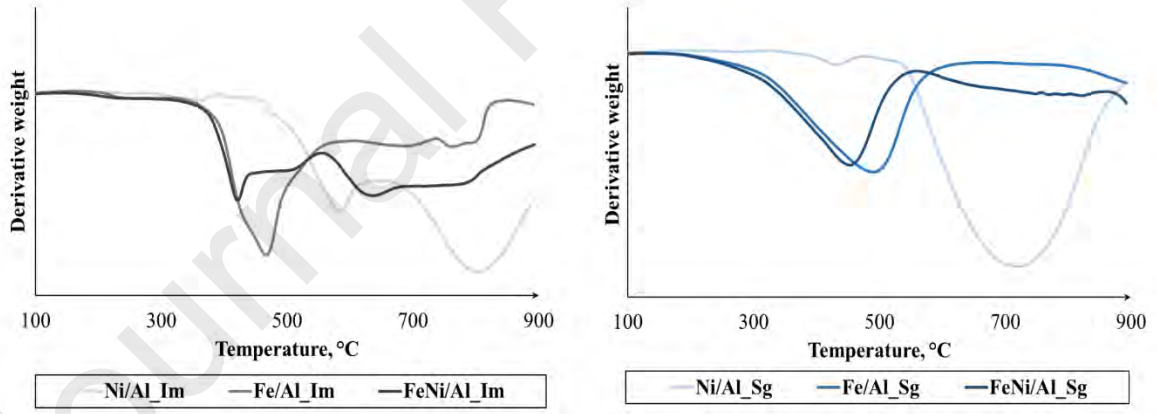

Fig. 3 TPR analysis for the fresh catalysts

3.2. Catalytic pyrolysis using different catalysts types

3.2.1. Product yields

The mass balances for pyrolysis using different types of catalyst and a reference case (Sand) are shown in Table 3. Additionally, Fig. 4 presents the yield values in a dry-ash free state (overlooking the inert-material

yield) to facilitate the comparison between the catalysts. In this case, a solid residue was divided into inert material (ash) and combustible material (char), whereas a carbon deposition on a catalyst was referred to as coke in the figure. The variation of inert material contents shown in Table 3 results from variations in feedstock composition, which are common in the case of waste.

The decrease of condensables yield in favour of non-condensables and coke deposition can be observed in the case of all analysed catalysts. Overall, the catalysts prepared using the sol-gel method show higher condensables yield reduction than those prepared using the impregnation method. The sol-gel catalysts also tend to yield higher coke yields than the impregnation catalysts, except for Fe/Al_Sg. This is because Fe/Al_Sg shows weaker metal-support interactions compared to the other catalysts (Fig. 3), which might cause the reduced formation of metal particles that could participate in the deposit formation [43,70]. This is in line with the findings of Yao et al. [22,23], where catalysts prepared using the impregnation method yielded higher condensables and lower coke yields than those prepared using the sol-gel method.

Among all the analysed catalysts, Ni/Al_Im yields the highest condensables amount and, consequently, the lowest non-condensables yield. This is in line with the findings of Acomb et al. [43] and Yao et al. [23,26], where among Ni- and Fe- based catalysts, Fe- catalysts show better overall performance in terms of condensables reduction in favour of non-condensables and coke.

The highest coke and non-condensables yields were obtained using the bimetallic catalysts (FeNi/Al_Im and FeNi/Al_Sg). Similar non-condensables yields characterise these two catalysts, but FeNi/Al_Sg outperformed FeNi/Al_Im with respect to the coke yield. The performance of the bimetallic catalysts might be related not only to its higher BET surface area and pore volume (Table 2) but also to its improved reducibility indicating higher activity in comparison to Fe- based catalysts, as seen in the TPR results (Fig. 3). Yao et al. [23] also observed higher coke yield when using a FeNi/Al_Sg catalyst compared to a FeNi/Al_Im catalyst and very similar non-condensables yields when using the sol-gel and impregnation Fe- and FeNi- catalysts.

Table 3 Pyrolysis product yields in a dry state for different catalysts

Yield, wt%	Sand	Ni_Im	Ni/Al_Sg	Fe/Al_Im	Fe/Al_Sg	FeNi/Al_Im	FeNi/Al_Sg
inert material	47.0±0.5	48.3±0.5	52.9±0.6	47.5±0.7	55.0±0.2	50.1±1.5	55.4±0.5
char	6.2±0.1	5.9±0.1	5.4±0.1	5.6±0.1	5.8±0.02	5.9±0.2	4.5±0.04
condensables	33.1±0.9	26.0±0.5	18.7±0.1	21.5±0.8	17.8±0.4	20.9±0.1	16.2±0.8
non-condensables	10.1±0.1	8.6±0.1	9.8±0.1	11.6±0.5	12.6±0.6	15.7±0.7	14.1±0.4
coke	3.4±0.2	8.0±0.7	9.0±0.2	11.1±0.3	4.9±0.1	4.5±0.01	8.0±0.5

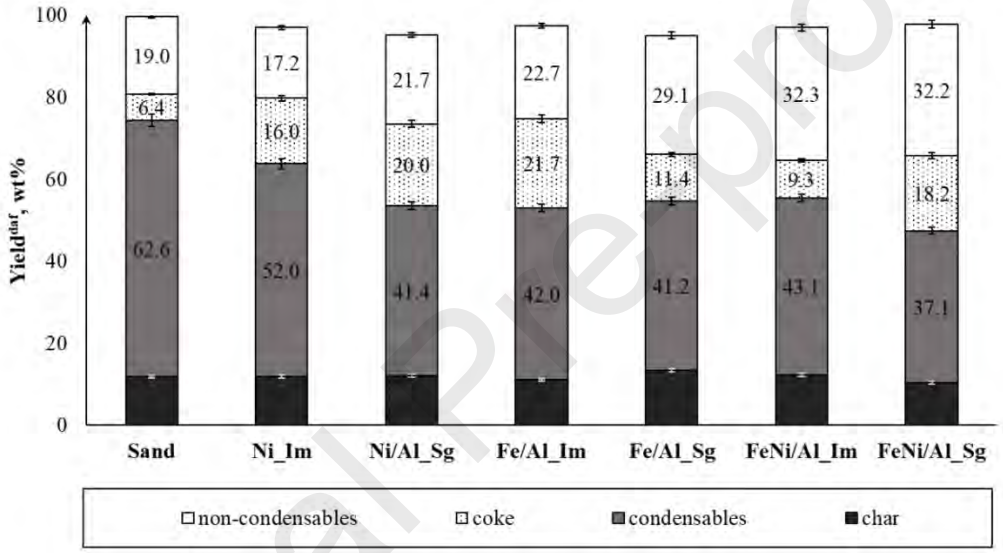

Fig. 4 Pyrolysis products yields in dry-ash free state for different catalysts

3.2.2. Non-condensables composition

The non-condensables composition for different catalysts is shown in Fig. 5. The exact values can be found in Table A1 in the Supplementary material. In addition, the H_2 yields and the H_2 conversion rates (fraction of an initial H_2 mass in the feedstock converted into H_2 gas) are presented in Table 4.

The H_2 content increase and the CH_4 and C_{2-4}-gases contents decrease, compared to the reference case (Sand), can be seen for all catalysts (Fig. 5). This tendency coincides with the findings of Acomb et al. [43] and Yao et al. [22,23] and indicates the catalytic decomposition of pyrovolatiles. Overall, the sol-gel catalysts outperform the impregnation ones, which is in line with the findings of Yao et al. [22] and is likely due to the

aforementioned improved reducibility (Fig. 3) and porosity (Table 2) of those catalysts. The highest hydrogen concentration was observed for Ni/Al_Sg, followed by the FeNi/Al_Sg catalyst (Fig. 5). However, the bimetallic catalyst shows a higher H_2 conversion rate than the Ni/Al_Sg catalyst (Table 4) because it yields a higher non-condensables amount (

Table 3). This might be related to the aforementioned Fe-Ni interactions (e.g., tuned carbon solubility) in the bimetallic catalyst improving reactions selectivity towards promoting the C-H bond dissociation and, consequently, intensifying the carbon deposition hydrogen release [23,79].

In general, the Fe/Al_Im outperforms the Ni/Al_Im catalyst in terms of H_2 yield and its conversion rate (Table 4). This tendency is in line with the findings of Acomb et al. [43] and Yao et al. [26] for the catalysts prepared with the same method and same metal loading. Similarly, Yao et al. [23] reported the Fe/Al_Sg catalyst's better performance than the Ni/Al_Sg catalyst. This was suggested to be due to a higher carbon solubility of Fe than that of Ni, which resulted in the intensified carbon deposition and, therefore, a higher H_2 yield as hydrogen is given off during carbon deposition [26,39]. Notwithstanding that, in the current study, the analysed Fe/Al_Sg catalyst shows a lower efficiency than that of the Ni/Al_Sg catalyst. This might be related to the aforementioned weaker metal-support bonds in the Fe/Al_Sg catalyst, which caused the detaching of metal particles from the support, their subsequent sintering, and, as a result, a decrease in the catalyst activity [70].

The obtained H_2 conversion rates (Table 4) are generally lower than those detected by Acomb et al. [43] for the in-line catalytic decomposition of pyrovapours from LDPE pyrolysis. Similarly, Yao et al. [27] obtained a higher H_2 yield when using a FeNi/Al_Im catalyst for the pyrolysis of plastic waste (predominantly polyolefins). This might result from the complex composition of the analysed feedstock and, consequently, a complex pyrovapours composition containing numerous compound types like, for instance, aromatic compounds and polycyclic aromatic hydrocarbons [21]. These are more difficult to reform than aliphatics from polyolefins pyrolysis [39]. In addition, it might be related to relatively high Cl and S contents in the feedstock, causing catalyst poisoning and, consequently, decreasing its efficiency [39,80].

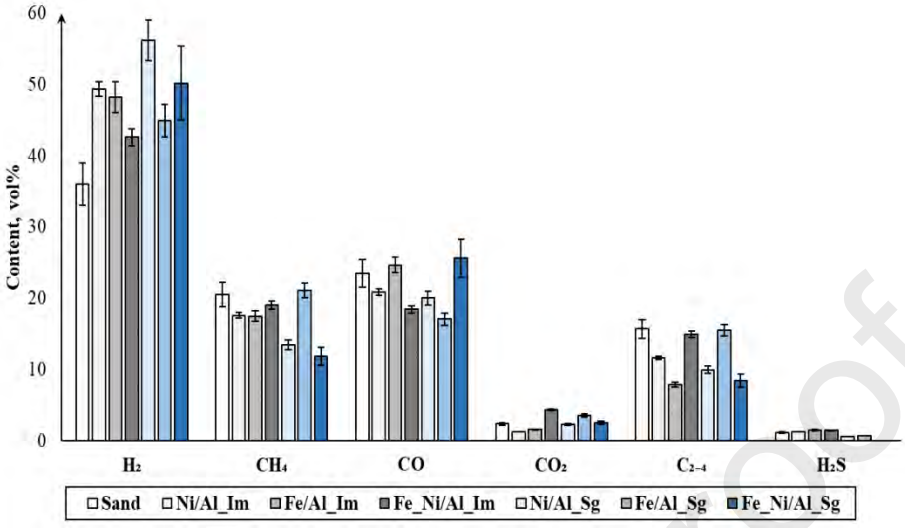

Fig. 5 The non-condensables composition for different catalysts

Table 4 H_2 and CNTs yields for different catalysts

	H_2 yield, mmol/g_{sample_daf}	**H_2 conversion ratio, wt%**	**CNTs yield, mg/g_{sample_daf}**
Sand	2.6±0.27	4.6	-
Ni/Al_Im	5.5±0.24	9.8	22
Ni/Al_Sg	7.8±0.48	12.5	82
Fe/Al_Im	6.6±0.28	11.5	31
Fe/Al_Sg	6.8±0.26	12.3	11
FeNi/Al_Im	7.7±0.73	13.5	47
FeNi/Al_Sg	9.0±0.23	15.7	76

3.2.3. Condensables chemical composition

Table 5 shows five main compounds found in the condensables, along with their contents altogether. The complete list of the identified compounds in the condensables can be found in Tables A2-3 in the Supplementary material.

The obtained condensables for the reference case (Sand) and for the cases using catalysts predominantly consist of polycyclic aromatic hydrocarbons (PAHs), where phenanthrene, pyrene, and fluoranthene dominate (Table 5). Their formation is likely due to the secondary Diels-Alder, dehydrogenation and condensation reactions triggered by the elevated temperatures [21,59,81]. As a mixture of low- and high-molecular-weight PAHs, the obtained condensables pose a considerable risk to the environment and, most likely, would have to be treated as hazardous waste [82,83].

High contents of PAHs among condensables are in line with the results reported in the study of Blanco et al. [84] on the RDF pyrolysis with catalytic steam reforming of the produced pyrovapours. However, the obtained results within this study show no catalysts' influence on the condensables composition, which does not coincide with the studies of Blanco et al. [84], Acomb et al. [28], and Zaini et al. [11]. Blanco et al. [84] detected cracking of pyrene and anthracene when using a Ni/Al_2O_3 catalyst. Similarly, Acomb et al. [28] observed intensified cracking of larger molecules (such as phenanthrene or benz[a]anthracene) to smaller aromatics over a catalyst during the steam reforming of pyrovapours from the pyrolysis of waste electrical and electronic equipment (WEEE). Furthermore, Zaini et al. [11] performed steam gasification of the same feedstock, which is used within this study (RDF formed from excavated waste), and obtained tars with mostly smaller aromatic compounds (toluene, xylenes, and naphthalene). This discrepancy between the current and the mentioned studies might be related to the presence of steam in the latter's case, which intensified the cracking of larger hydrocarbons over the used catalysts.

Table 5 The main components detected in the condensables

	Sand	**Ni/Al_Im**	**Ni/Al_Sg**	**Fe/Al_Im**	**Fe/Al_Sg**	**FeNi/Al_Im**	**FeNi/Al_Sg**
	phenanthrene	phenanthrene	phenanthrene	pyrene	phenanthrene	phenanthrene	phenanthrene
	pyrene	pyrene	pyrene	phenanthrene	pyrene	pyrene	pyrene
	fluoranthene	fluoranthene	fluoranthene	fluoranthene	fluoranthene	fluoranthene	fluoranthene
	benz[a]anthracene	naphthalene	naphthalene	benz[a]anthracene	anthracene	biphenylene	anthracene
	anthracene	anthracene	biphenylene	naphthalene	perylene	anthracene	benz[a]anthracene
Content altogether, weight-normalised area%	66.7	65.1	74.1	89.9	65.1	61.6	75.4

3.2.4. Carbon deposition characterisation

The carbon depositions on the catalysts were characterised using temperature-programmed oxidation (TPO) and Raman spectroscopy (Fig. 6). The I_D/I_G and $I_{G'}/I_G$ ratios calculated from the Raman spectra can be found in Table A4 in the Supplementary material. The yields of CNTs, calculated based on the TPO analysis, are presented in Table 4. Additionally, the spent catalyst with the highest carbon deposit quality was examined using FE-SEM, and the result is shown in Fig. A4 in the Supplementary material.

Raman spectroscopy was used to study the graphitisation degree of the carbon deposits (Fig. 6a-b). The so-called D (a wavelength of ~1350 cm^{-1}) and G (a wavelength of ~1600 cm^{-1}) peaks can be seen for all catalysts. Additionally, in some of the catalysts' spectra, the so-called D' (a shoulder of the G peak) and a G' band (a wavelength of ~2700 cm^{-1}) can be seen. The D band and its sister band D' are related to the structural defects of graphite or amorphous carbon, the G band is a graphitic band, whereas the G' band can be used to estimate the purity of the deposited carbon [85]. For assessing the graphitisation degree of the carbon deposits, the intensity I_D/I_G ratio is used, whereas the $I_{G'}/I_G$ ratio is used to evaluate the degree of graphite crystallinity [86]. In addition, the thermal oxidation patterns of the spent catalysts were studied using TPO (Fig. 6c-d) to complement the Raman analysis, as peaks occurring at temperatures below 500ºC are associated with amorphous coke, whereas those at above 500ºC correspond to filamentous coke [58]. Moreover, for some catalysts (Ni/Al_Sg, FeNi/Al_Sg, FeNi/Al_Im), an increase in mass can be seen in TPO, indicating the oxidation of remaining Ni at their surface [87].

The catalysts prepared using the sol-gel method are generally characterised by lower I_D/I_G ratios than that of the impregnation catalysts, indicating less disordered carbon in their case. Moreover, the Ni/Al_Sg and FeNi/Al_Sg catalysts show well-pronounced peaks in the TPO profile at temperatures around 600ºC (Fig. 6d), confirming the presence of filamentous carbon. The lowest I_D/I_G ratio (0.92) among all analysed catalysts occurs in the case of the FeNi/Al_Sg catalyst, whereas its $I_{G'}/I_G$ ratio is 0.89. Additionally, the FE-SEM analysis confirmed the presence of dense, entangled filamentous carbon structures at the FeNi/Al_Sg surface, which length was up to several microns (Fig. A4 in the Supplementary material).

On the contrary, the Fe/Al_Sg Raman spectrum does not show the G' band (Fig. 6b), indicating somewhat disordered carbon deposition on this catalyst [85]. Those results are in line with the observations of

Nahil et al. [86], where the catalysts with higher BET surface areas resulted in the formation of more filamentous coke. The lower carbon deposit quality at Fe/Al_Sg might also be related to the aforementioned weaker metal-support interactions, causing detaching of metal particles from the support, their sintering, and thus decreasing the catalyst activity [70]. Last but not least, the obtained I_D/I_G ratios are in the same range as in the study of Yao et al. [26], in which the same types of catalysts were used.

Among the catalysts prepared using the impregnation method, only the Ni/Al_Im Raman spectrum shows a pronounced G' band (Fig. 6a), indicating a more disordered structure of the deposits at the other two catalysts (Fe/Al_Im, FeNi/Al_Im). Moreover, the TPO analysis of the Ni/Al_Im yielded one pronounced peak at around 660ºC (Fig. 6c), confirming the presence of filamentous coke. However, its I_D/I_G ratio is relatively high (1.35), which indicates that a considerable amount of amorphous coke is also present on the catalyst surface [86]. Similarly, in the case of the Fe/Al_Im and FeNi/Al_Im catalysts, the TPO profiles indicate the presence of both amorphous and filamentous coke, as is reflected by two peaks at around 440ºC and 700ºC (Fe/Al_Im) or one flat overlapping peak starting below 450ºC (FeNi/Al_Im). Likewise, the TPO profile of the FeNi/Al_Im comprises one prolonged flat peak being overlapping peaks.

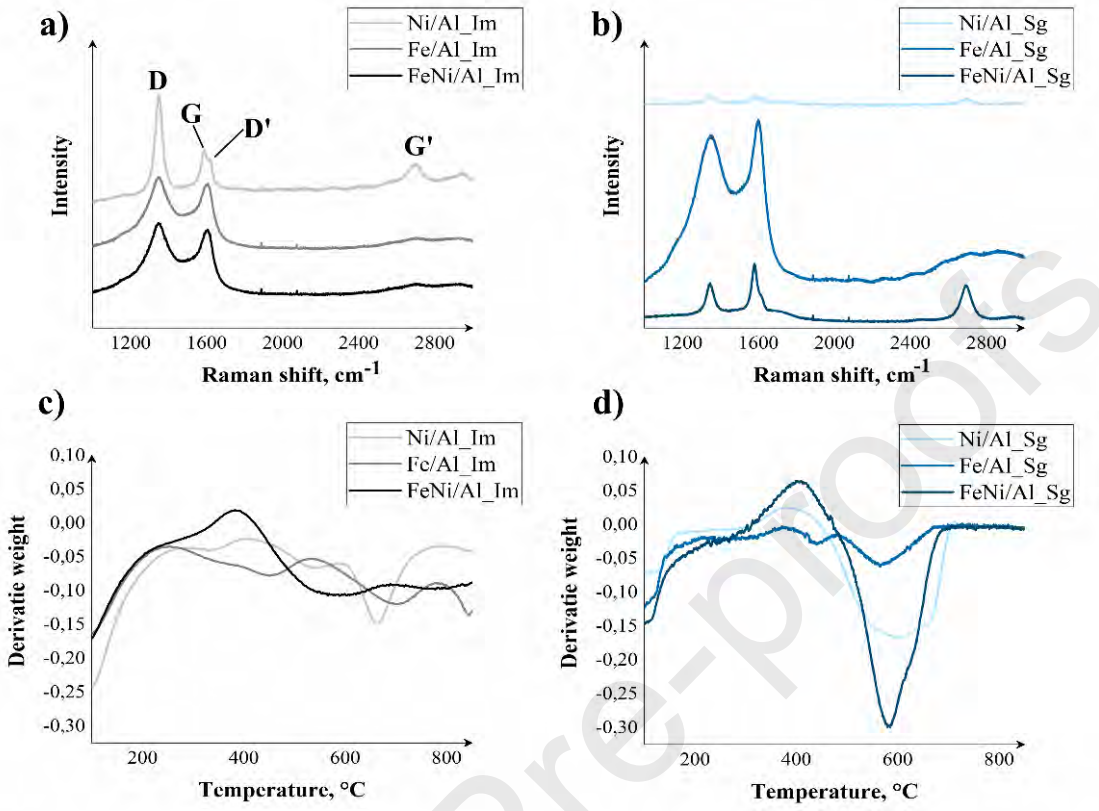

Fig. 6 The Raman spectra of carbon depositions (a,b) and TPO results (c,d) for different catalysts

3.3. Catalytic pyrolysis at different catalyst bed temperatures

The FeNi/Al_Sg catalyst was chosen to further investigate the influence of the catalytic bed temperature on the process products. This is because it outperformed other analysed catalysts with respect to the H_2 yield and H_2 conversion rate as well as showed one of the highest CNTs yields (Table 4).

Fig. 7 shows the process product yields in a dry-ash free state (overlooking the inert-material yield) for pyrolysis using the FeNi/Al_Sg catalyst at different catalytic bed temperatures. The exact values of product yields are shown in Table A5 in the Supplementary material.

No significant difference between product yields formed with the catalyst at 700°C and the reference case without catalyst can be observed (Fig. 7). This indicates the low activity of the catalyst at this temperature. On the contrary, the catalytic decomposition combined with thermal cracking occurs at 900°C; however, lower non-condensables and coke yields are formed compared to the process performed at 800°C. The decrease of the

non-condensables yield at higher temperatures was also observed by Acomb et al. [48], and the intensification of coke deposition followed it. However, no such intensification was observed in this study (Fig. 7; Table 6), which might be related to the sintering of metal particles at higher temperatures, resulting in decreased carbon deposition yields [88].

To investigate the reason behind the non-condensables yield decrease, additional tests were performed at a higher catalytic bed temperature (900°C) using sand instead of catalyst. The tests showed a similar non-condensables yield (9.6±0.5wt%) to the case with a catalyst used (Fig. 7). Therefore, it can be concluded that at 900°C thermal cracking is the main cause of non-condensables yield increase. When comparing the non-condensables yield at 900°C to that at 800°C, it is lower than at 800°C because, at 800°C, catalyst cracking takes place, which is more intensive than thermal cracking alone.

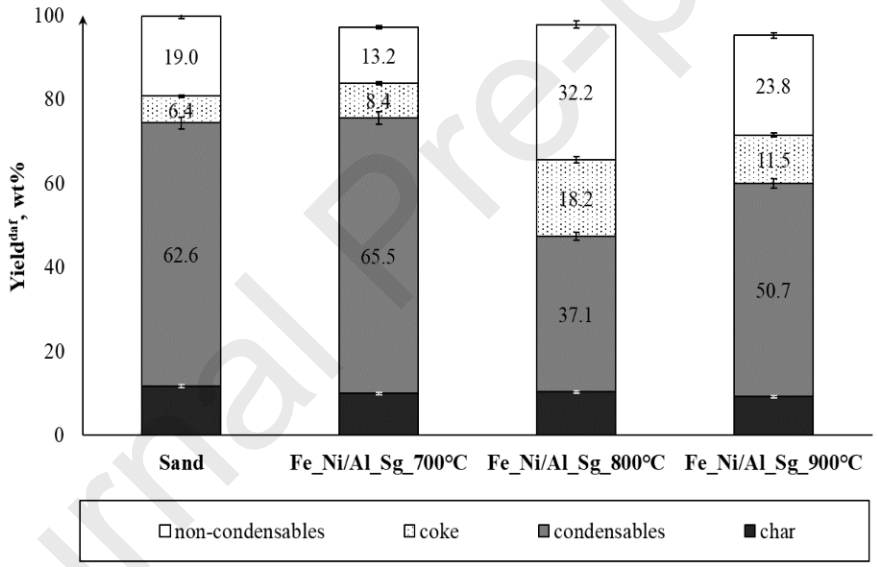

Fig. 7 Pyrolysis products yields in dry-ash free state for the FeNi/Al_Sg catalyst at different catalytic bed temperatures

Similarly, the low activity of the catalyst at 700°C is reflected in the non-condensables chemical composition (Fig. 8). More specifically, it has a lower H_2 yield and higher CH_4 and C_{2-4}-gases yields than the reference case without catalyst (Sand). The highest reduction in CH_4 and the light hydrocarbon gases (C_{2-4}-gases) can be seen at 800°C. Moreover, a high C_{2-4}-gases yield (Fig. 8) and a relatively high H_2 conversion ratio

at 900°C (Table 6) are likely related to both catalytic decomposition as well as thermal cracking at elevated temperatures [89].

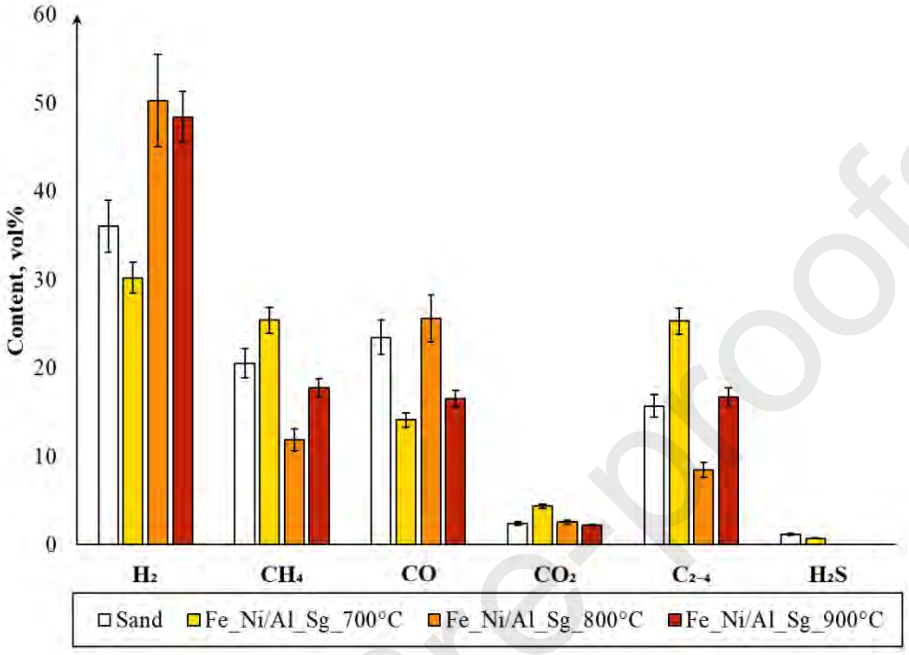

Fig. 8 The non-condensables composition for the FeNi/Al_Sg at different catalyst bed temperatures

Table 6 H_2 and CNTs yields at different catalyst bed temperatures

	H_2 yield, mmol/g_{sample_daf}	**H_2 conversion ratio, wt%**	**CNTs yield, mg/g_{sample_daf}**
Sand	2.6±0.27	4.6	-
FeNi/Al_Sg_700°C	1.8±0.10	3.0	29
FeNi/Al_Sg_800°C	9.0±0.23	15.7	76
FeNi/Al_Sg_900°C	6.6±0.36	11.7	3

The results of the characterisation of carbon deposits at different catalyst bed temperatures using Raman spectroscopy and TPO are shown in Fig. 9. It can be observed that the graphitisation degree of carbon deposits is the highest at 800°C, which is represented by a well-pronounced G' bond in a Raman spectrum and a lower I_D/I_G ratio (Fig. 9a). Moreover, with an increased temperature, the quality of the carbon deposition decreases,

which is reflected by a shifting of a TPO peak towards lower temperatures around 400°C (Fig. 9b). Consequently, at 900°C, the CNTs yield is the lowest (Table 6). This tendency coincides with the observations of Acomb et al. [48] and Yao et al. [26], who observed higher CNTs yields at 800°C than at 700°C, and detected a decrease in CNTs quality (crystallinity) at 900°C.

In light of the foregoing, it can be concluded that the initially chosen catalyst bed temperature of 800°C is optimal when using a FeNi/Al_Sg catalyst.

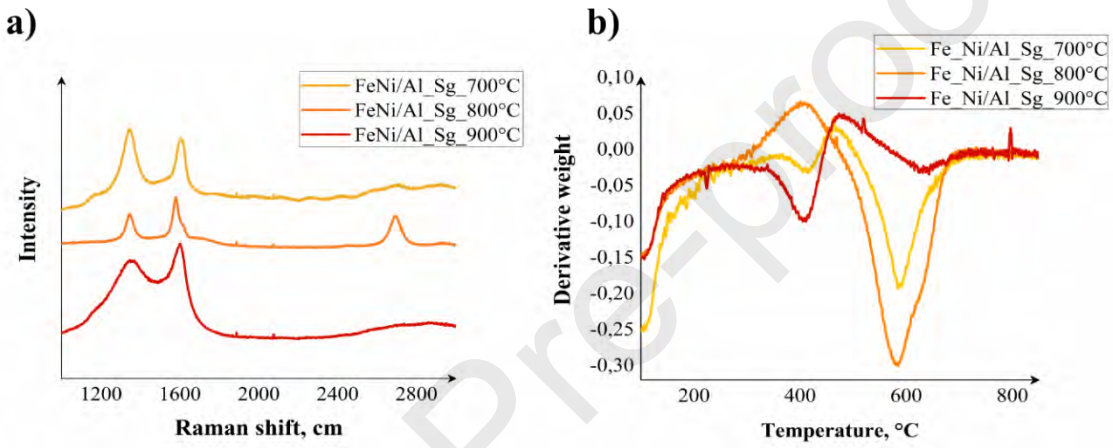

Fig. 9 The Raman spectra of carbon depositions (a) and TPO results (b) for the FeNi/Al_Sg catalyst at different catalyst bed temperatures

3.4. Discussion on possible further research directions

The main aim of this study was to investigate the possibility of producing a hydrogen-rich gas and CNTs from excavated waste using pyrolysis followed by the in-line catalytic decomposition of the pyrovapours. It was done to explore an additional way of excavated waste valorisation, which might complement gasification. A consensus on those two technologies' technical and economic potential has not yet been reached, and contrary statements on their feasibility can be found in the open literature [57,59]. Therefore, this study constitutes a starting point for the initial comparative analysis of those two processes and further research on their optimisation.

Within this study, the bimetallic catalyst synthesised using the sol-gel method (FeNi/Al_Sg) is proposed to be used in a further investigation as it overperformed the other studied catalysts. It yielded 0.15 g/g_{sample_daf} of non-condensables with the H_2/CO ratio of 2, the H_2 content of 50vol%, and a lower heating value (LHV) of 18 MJ/Nm^3. On the contrary, Zaini et al. [11] performed steam gasification of the same feedstock (RDF formed from excavated waste) at 800°C, which resulted in significantly higher syngas yield (around 0.75 g/g_{sample_daf} with the H_2 content of 38vol%) characterised by a higher H_2/CO ratio (2.5) and LHV of 24 MJ/Nm^3. Notwithstanding that, pyrolysis with in-line catalytic decomposition of the pyrovapours results in the formation of carbon nanotubes (CNTs), constituting an additional value, which shall be taken into account while assessing the process' feasibility. The FeNi/Al_Sg catalyst yielded 76 mg/g_{sample_daf} of CNTs with promising characteristics (I_D/I_G = 0.92) comparable to commercially used CNTs (I_D/I_G = 0.2-2.0) [27,85,90].

The obtained H_2 and CNTs yields (0.02 g/g_{sample_daf} and 76 mg/g_{sample_daf}, respectively) are, in general, lower but still comparable to those found in the open literature. As an example, Yao et al. [27] performed pyrolysis of mixed plastics with the subsequent catalytic decomposition of the produced pyrovapours using a FeNi/Al_Im catalyst, which resulted in 460 mg/g_{sample_daf} of CNTs and 0.085 g/g_{sample_daf} of H_2. Acomb et al. [88] performed LDPE and PS pyrolysis over a Ni/Al_Im catalyst and obtained 188 mg/g_{sample_daf} of CNTs with 0.033 g/g_{sample_daf} of H_2 for LDPE and 96 mg/g_{sample_daf} of CNTs with 0.027 g/g_{sample_daf} of H_2 for PS. In another study, Acomb et al. [48] performed LDPE pyrolysis and catalytic decomposition of the pyrovapours using a Fe/Al_Im catalyst, which yielded around 175 mg/g_{sample_daf} of CNTs and 0.039 g/g_{sample_daf} of H_2. On the contrary, Zhang et al. [91] obtained only 0.015 g/g_{sample_daf} of H_2 from waste tires pyrolysis using Fe/Al_Im catalyst. However, the H_2 yield was doubled when using Ni/Al_Im catalyst.

Given the above, it can be concluded that the feedstock composition and the catalyst type are crucial for the process performance. Therefore, the lower process efficiency in the current study might be related to the feedstock's heterogeneity, which is reflected in the complex composition of the produced pyrovapours. This, in turn, has an adverse effect on the catalyst activity. Moreover, the analysed feedstock is characterised by relatively high contents of sulphur and chlorine, which cause catalyst poisoning and thus decrease its activity [39,80]. Nevertheless, a margin for improvement regarding the process's efficiency can still be identified.

In the open literature, multiple ways of improving the efficiency of pyrolysis with in-line catalytic decomposition can be found. Firstly, a feedstock/catalyst ratio and parameters of catalyst calcination (atmosphere and temperature) play a crucial role in the process performance [48,86,92]. Secondly, in this study, catalysts were not reduced prior to the test as it was assumed that the reduction would occur in-situ by pyrovapours. However, in further process development, the reduction of catalysts before the process shall be considered as well as it might also increase CNTs yield [52,93] by improving catalyst activity [94]. Moreover, according to Yao et al. [70], increased H_2 and CNTs yields can be caused by changing the catalyst support to a highly porous (e.g., MCM41) or altering the catalyst composition by adding other metals (e.g., Co [43,72]). This porous structure results in a fine distribution of active species among the support, which improves the catalyst's activity. Furthermore, the quality of CNTs can be enhanced by increasing the Ni content in the bimetallic catalyst (leading to smoother and longer CNTs [27]) or by increasing the reaction pressure [95]. Also, the collection of produced CNTs can become easier when changing the catalyst support to, for instance, stainless steel mesh [24,52]. Finally, following Erkiaga et al. [57], commercial catalysts show better performance compared to those synthesised in the lab using a simplified methodology; therefore, the usage of commercial catalysts likely would increase the process' efficiency.

Adding steam to the process might be another way of enhancing its performance, even though it might increase the process's operational costs and decrease the CNTs yield [48]. However, according to Wu et al. [96], this CNTs yield decrease is also connected with improving the product quality. This is because adding steam to the process causes a considerable reduction of amorphous coke (of around 7 times), while filamentous coke is reduced less intensively (the reduction of around 2 times) [96]. The same tendency was observed by Xu et al. [97] when adding steam to the co-gasification of biomass and plastic waste.

The synthesis of pure and untangled CNTs remains challenging, hindering their use in various industries on a larger scale [31,52]. Therefore, improvement of CNTs quality should also be considered while planning further process development, even though the following purification step is often required in all CNTs production techniques (i.e., chemical vapour deposition, laser-ablation and arc-discharge) [31]. Last but not least, one of the biggest obstacles related to the thermochemical processing of waste is the tar presence in the

obtained gas, hindering its utilisation in downstream applications [98,99]. Therefore, the purification of the obtained gas (i.e., tar and undesirable gases removal) shall also be taken into account in further research.

To sum up, there is an apparent need for further research on excavated waste pyrolysis with the in-line catalytic decomposition of pyrovapours, focusing on improving the process efficiency. As discussed above, numerous ways of enhancing the activity of the catalysts can be found in the open literature, such as, for example, modifying catalyst composition and its synthesis method, reaction pressure, or, eventually, adding steam to the process.

4. Conclusions

The study aimed to investigate the possibility and potential of producing carbon nanotubes (CNTs) and hydrogen rich-gas from excavated landfill waste. It was performed by subjecting the waste to pyrolysis followed by catalytic decomposition of the formed pyrovapours. The investigation covered the impact of the catalyst composition, its synthesis method, and the catalyst bed temperature on the process products' qualities.

The specific findings of the study can be summarised as follows:

1. The catalysts synthesised using the sol-gel method outperform the impregnation ones, both in terms of their properties (porosity and reducibility) and the H_2 and CNTs yields.
2. The bimetallic catalysts outperform the monometallic ones, which is related to the Fe-Ni interactions (Fe-Ni alloy), promoting the catalyst's selectivity towards C-H bond dissociation, thereby intensifying carbon deposition and hydrogen release.
3. The FeNi/Al_Sg catalyst yielded the highest CNTs and non-condensables amounts with the highest H_2 conversion rates being more than three times higher than that of the reference case (no catalyst).
4. The performance of the FeNi/Al_Sg catalyst is optimal at a catalytic bed temperature of 800°C.

Overall, this novel study demonstrates that excavated waste pyrolysis can yield comparable qualities and amounts of CNTs and H_2 as those from homogeneous plastic waste pyrolysis, despite the complex composition of the excavated waste and its high contamination. Consequently, it can be concluded that the process has the potential to tackle the environmental risks posed by non-sanitary landfills and simultaneously provide society with highly valuable products necessary for the transition to a more sustainable future.

However, as the presented concept is emerging, it naturally requires further investigations and developments, and there are numerous possible directions for future work. Based on the performed study, however, three main optimisation parameters are suggested for further investigations:

- catalyst composition (e.g., changing the catalyst support),
- catalyst preparation method (e.g., changing calcination temperature or atmosphere),
- process parameters (e.g., a catalyst/sample ratio or the process pressure).

CRediT authorship contribution statement

Katarzyna Jagodzińska: Conceptualization, Methodology, Investigation, Writing - original draft, Writing-review & editing. **Pär Göran Jönsson**: Supervision, Writing-review & editing. **Weihong Yang**: Supervision, Writing-review & editing.

Acknowledgement

The research was performed within the NEW-MINE project, which has received funding from the European Union's Horizon 2020 research and innovation programme under the Marie Sklodowska-Curie grant agreement No 721185. The project website is http://new-mine.eu/. K. Jagodzińska would also like to thank Jernkontoret for the financial support and acknowledge the help received from Tong Han and Hanmin Yang.

References

[1] A. Winterstetter, S. Heuss-Assbichler, J. Stegemann, U. Kral, P. Wäger, M. Osmani, H. Rechberger, The role of anthropogenic resource classification in supporting the transition to a circular economy, J. Clean. Prod. 297 (2021). https://doi.org/10.1016/j.jclepro.2021.126753.

[2] P.T. Jones, D. Geysen, Y. Tielemans, S. Van Passel, Y. Pontikes, B. Blanpain, M. Quaghebeur, N. Hoekstra, Enhanced Landfill Mining in view of multiple resource recovery: A critical review, J. Clean. Prod. 55 (2013) 45–55. https://doi.org/10.1016/j.jclepro.2012.05.021.

[3] D. Laner, J.L. Esguerra, J. Krook, M. Horttanainen, M. Kriipsalu, R.M. Rosendal, N. Stanisavljević, Systematic assessment of critical factors for the economic performance of landfill mining in Europe: What drives the economy of landfill mining?, Waste Manag. 95 (2019) 674–686. https://doi.org/10.1016/j.wasman.2019.07.007.

[4] M. Quaghebeur, B. Laenen, D. Geysen, P. Nielsen, Y. Pontikes, T. Van Gerven, J. Spooren, Characterization of landfilled materials: screening of the enhanced landfill mining potential, J. Clean. Prod. 55 (2013) 72–83. https://doi.org/10.1016/j.jclepro.2012.06.012.

[5] C. Zhou, W. Fang, W. Xu, A. Cao, R. Wang, Characteristics and the recovery potential of plastic wastes obtained from landfill mining, J. Clean. Prod. 80 (2014) 80–86. https://doi.org/10.1016/j.jclepro.2014.05.083.

[6] J. Burlakovs, M. Kriipsalu, M. Klavins, A. Bhatnagar, Z. Vincevica-Gaile, J. Stenis, Y. Jani, V. Mykhaylenko, G. Denafas, T. Turkadze, M. Hogland, V. Rudovica, F. Kaczala, R.M. Rosendal, W. Hogland, Paradigms on landfill mining: From dump site scavenging to ecosystem services revitalization, Resour. Conserv. Recycl. 123 (2017) 73–84. https://doi.org/10.1016/j.resconrec.2016.07.007.

[7] O. Eriksson, G. Finnveden, Plastic waste as a fuel - CO2-neutral or not?, Energy Environ. Sci. 2 (2009) 907–914. https://doi.org/10.1039/b908135f.

[8] A. Bosmans, I. Vanderreydt, D. Geysen, L. Helsen, The crucial role of Waste-to-Energy technologies in enhanced landfill mining: A technology review, J. Clean. Prod. 55 (2013) 10–23. https://doi.org/10.1016/j.jclepro.2012.05.032.

[9] M. Danthurebandara, S. Van Passel, I. Vanderreydt, K. Van Acker, Environmental and economic performance of plasma gasification in Enhanced Landfill Mining, Waste Manag. 45 (2015) 458–467. https://doi.org/10.1016/j.wasman.2015.06.022.

[10] N. Agon, M. Hrabovský, O. Chumak, M. Hlína, V. Kopecký, A. Mašláni, A. Bosmans, L. Helsen, S. Skoblja, G. Van Oost, J. Vierendeels, Plasma gasification of refuse derived fuel in a single-stage system using different gasifying agents, Waste Manag. 47 (2016) 246–255. https://doi.org/10.1016/j.wasman.2015.07.014.

[11] I.N. Zaini, Y. Gomez-Rueda, C. García López, D.K. Ratnasari, L. Helsen, T. Pretz, P.G. Jönsson, W. Yang, Production of H2-rich syngas from excavated landfill waste through steam co-gasification with biochar, Energy. 207 (2020). https://doi.org/10.1016/j.energy.2020.118208.

[12] I.N. Zaini, C. García López, T. Pretz, W. Yang, P.G. Jönsson, Characterization of pyrolysis products of high-ash excavated-waste and its char gasification reactivity and kinetics under a steam atmosphere, Waste Manag. 97 (2019) 149–163. https://doi.org/10.1016/j.wasman.2019.08.001.

[13] I.N. Zaini, W. Yang, P.G. Jönsson, Steam gasification of solid recovered fuel char derived from landfill waste: A kinetic study, Energy Procedia. 142 (2017) 723–729. https://doi.org/10.1016/j.egypro.2017.12.118.

[14] J.L. Esguerra, J. Krook, N. Svensson, S. Van Passel, ASSESSING THE ECONOMIC POTENTIAL OF LANDFILL MINING : REVIEW AND RECOMMENDATIONS, Detritus. 08 (2019) 125–140. https://doi.org/10.31025/2611-4135/2019.13883.

[15] M. Danthurebandara, S. Van Passel, I. Vanderreydt, K. Van Acker, Assessment of environmental and economic feasibility of Enhanced Landfill Mining, Waste Manag. 45 (2014) 434–447. https://doi.org/10.1016/j.wasman.2015.01.041.

[16] L. Canopoli, B. Fidalgo, F. Coulon, S.T. Wagland, Physico-chemical properties of excavated plastic from landfill mining and current recycling routes, Waste Manag. 76 (2018) 55–67. https://doi.org/10.1016/j.wasman.2018.03.043.

[17] L. Canopoli, F. Coulon, S.T. Wagland, Degradation of excavated polyethylene and polypropylene waste from landfill, Sci. Total Environ. 698 (2020) 134125. https://doi.org/10.1016/j.scitotenv.2019.134125.

[18] S. Ciuta, D. Tsiamis, M.J. Castaldi, Field scale developments, in: Gasif. Waste Mater. Technol. Gener. Energy, Gas, Chem. from Munic. Solid Waste, Biomass, Nonrecycled Plast. Sludges, Wet Solid Wastes, 2017: pp. 65–91. https://doi.org/10.1016/B978-0-12-812716-2.00004-2.

[19] S. Ciuta, D. Tsiamis, M.J. Castaldi, Economic summary, in: Gasif. Waste Mater. Technol. Gener. Energy, Gas, Chem. from Munic. Solid Waste, Biomass, Nonrecycled Plast. Sludges, Wet Solid Wastes, 2017: pp. 143–150. https://doi.org/10.1016/B978-0-12-812716-2.00007-8.

[20] B. Baytekin, H.T. Baytekin, B.A. Grzybowski, Retrieving and converting energy from polymers: Deployable technologies and emerging concepts, Energy Environ. Sci. 6 (2013) 3467–3482. https://doi.org/10.1039/c3ee41360h.

[21] K. Jagodzińska, I.N. Zaini, R. Svanberg, W. Yang, P.G. Jönsson, Pyrolysis of excavated waste from landfill mining: Characterisation of the process products, J. Clean. Prod. 279 (2021). https://doi.org/10.1016/j.jclepro.2020.123541.

[22] D. Yao, H. Yang, H. Chen, P.T. Williams, Co-precipitation, impregnation and so-gel preparation of Ni catalysts for pyrolysis-catalytic steam reforming of waste plastics, Appl. Catal. B Environ. 239 (2018) 565–577. https://doi.org/10.1016/j.apcatb.2018.07.075.

[23] D. Yao, C.H. Wang, Pyrolysis and in-line catalytic decomposition of polypropylene to carbon nanomaterials and hydrogen over Fe- and Ni-based catalysts, Appl. Energy. 265 (2020) 114819. https://doi.org/10.1016/j.apenergy.2020.114819.

[24] Y. Zhang, M.A. Nahil, C. Wu, P.T. Williams, Pyrolysis-catalysis of waste plastic using a nickel-stainless steel mesh catalyst for high value carbon products, Environ. Technol. 38 (2017) 2889–2897. https://doi.org/10.1080/09593330.2017.1281351.

[25] X. Liu, B. Shen, P. Yuan, D. Patel, C. Wu, Production of carbon nanotubes (CNTs) from thermochemical conversion of waste plastics using Ni / anodic aluminum oxide (AAO) template catalyst, in: Energy Procedia, Elsevier B.V., 2017: pp. 525–530. https://doi.org/10.1016/j.egypro.2017.12.082.

[26] D. Yao, Y. Zhang, P.T. Williams, H. Yang, H. Chen, Co-production of hydrogen and carbon nanotubes from real-world waste plastics: Influence of catalyst composition and operational parameters, Appl.

Catal. B Environ. 221 (2018) 584–597. https://doi.org/10.1016/j.apcatb.2017.09.035.

[27] D. Yao, C. Wu, H. Yang, Y. Zhang, M.A. Nahil, Y. Chen, P.T. Williams, H. Chen, Co-production of hydrogen and carbon nanotubes from catalytic pyrolysis of waste plastics on Ni-Fe bimetallic catalyst, Energy Convers. Manag. 148 (2017) 692–700. https://doi.org/10.1016/j.enconman.2017.06.012.

[28] J.C. Acomb, M.A. Nahil, P.T. Williams, Thermal processing of plastics from waste electrical and electronic equipment for hydrogen production, J. Anal. Appl. Pyrolysis. 103 (2013) 320–327. https://doi.org/10.1016/j.jaap.2012.09.014.

[29] I. Kremer, T. Tomić, Z. Katančić, Z. Hrnjak-Murgić, M. Erceg, D.R. Schneider, Catalytic decomposition and kinetic study of mixed plastic waste, Clean Technol. Environ. Policy. 23 (2021) 811–827. https://doi.org/10.1007/s10098-020-01930-y.

[30] S. Rai, A. Ikram, S. Sahai, S. Dass, R. Shrivastav, V.R. Satsangi, CNT based photoelectrodes for PEC generation of hydrogen: A review, Int. J. Hydrogen Energy. 42 (2017) 3994–4006. https://doi.org/10.1016/j.ijhydene.2016.10.024.

[31] S.K. Soni, B. Thomas, V.R. Kar, A Comprehensive Review on CNTs and CNT-Reinforced Composites: Syntheses, Characteristics and Applications, Mater. Today Commun. 25 (2020). https://doi.org/10.1016/j.mtcomm.2020.101546.

[32] N. Jain, S. Tiwari, Biomedical application of carbon nanotubes (CNTs) in vulnerable parts of the body and its toxicity study: A state-of-the-art-review, Mater. Today Proc. (2021). https://doi.org/10.1016/j.matpr.2021.01.895.

[33] P.M. Falcone, M. Hiete, A. Sapio, Hydrogen economy and Sustainable Development Goals (SDGs): Review and policy insights, Curr. Opin. Green Sustain. Chem. (2021) 100506. https://doi.org/10.1016/j.cogsc.2021.100506.

[34] S.N. Reddy, S. Nanda, D.-V.N. Vo, T.D. Nguyen, V.-H. Nguyen, B. Abdullah, P. Nguyen-Tri, Hydrogen: fuel of the near future, in: New Dimens. Prod. Util. Hydrog., INC, 2020: pp. 1–20. https://doi.org/10.1016/b978-0-12-819553-6.00001-5.

[35] A. Bazargan, G. McKay, A review - Synthesis of carbon nanotubes from plastic wastes, Chem. Eng. J. 195–196 (2012) 377–391. https://doi.org/10.1016/j.cej.2012.03.077.

[36] G. Lota, K. Fic, E. Frackowiak, Carbon nanotubes and their composites in electrochemical applications, Energy Environ. Sci. 4 (2011) 1592–1605. https://doi.org/10.1039/c0ee00470g.

[37] C. Jin, J. Nai, O. Sheng, H. Yuan, W. Zhang, X. Tao, X.W. Lou, Biomass-based materials for green lithium secondary batteries, Energy Environ. Sci. 14 (2021) 1326–1379. https://doi.org/10.1039/d0ee02848g.

[38] M. Sevilla, R. Mokaya, Energy storage applications of activated carbons: Supercapacitors and hydrogen storage, Energy Environ. Sci. 7 (2014) 1250–1280. https://doi.org/10.1039/c3ee43525c.

[39] P.T. Williams, Hydrogen and Carbon Nanotubes from Pyrolysis-Catalysis of Waste Plastics: A Review, Waste and Biomass Valorization. 12 (2021) 1–28. https://doi.org/10.1007/s12649-020-01054-w.

[40] M.M. Khin, A.S. Nair, V.J. Babu, R. Murugan, S. Ramakrishna, A review on nanomaterials for environmental remediation, Energy Environ. Sci. 5 (2012) 8075–8109. https://doi.org/10.1039/c2ee21818f.

[41] C. Wu, M.A. Nahil, N. Miskolczi, J. Huang, P.T. Williams, Production and application of carbon nanotubes, as a co-product of hydrogen from the pyrolysis-catalytic reforming of waste plastic, Process Saf. Environ. Prot. 103 (2016) 107–114. https://doi.org/10.1016/j.psep.2016.07.001.

[42] K. Akubo, M.A. Nahil, P.T. Williams, Pyrolysis-catalytic steam reforming of agricultural biomass wastes and biomass components for production of hydrogen/syngas, J. Energy Inst. (2018). https://doi.org/10.1016/j.joei.2018.10.013.

[43] J.C. Acomb, C. Wu, P.T. Williams, The use of different metal catalysts for the simultaneous production of carbon nanotubes and hydrogen from pyrolysis of plastic feedstocks, Appl. Catal. B Environ. 180 (2016) 497–510. https://doi.org/10.1016/j.apcatb.2015.06.054.

[44] C. He, N. Zhao, Y. Han, J. Li, C. Shi, X. Du, Study of aluminum powder as transition metal catalyst carrier for CVD synthesis of carbon nanotubes, Mater. Sci. Eng. A. 441 (2006) 266–270. https://doi.org/10.1016/j.msea.2006.08.072.

[45] P.H. Blanco, C. Wu, J.A. Onwudili, P.T. Williams, Characterization and evaluation of Ni/SiO2 catalysts for hydrogen production and tar reduction from catalytic steam pyrolysis-reforming of refuse derived fuel, Appl. Catal. B Environ. 134–135 (2013) 238–250. https://doi.org/10.1016/j.apcatb.2013.01.016.

[46] C. Wu, P.T. Williams, Pyrolysis – gasification of post-consumer municipal solid plastic waste for hydrogen production, Int. J. Hydrogen Energy. 35 (2010) 949–957. https://doi.org/10.1016/j.ijhydene.2009.11.045.

[47] X. Liu, Y. Zhang, M.A. Nahil, P.T. Williams, C. Wu, Development of Ni- and Fe- based catalysts with different metal particle sizes for the production of carbon nanotubes and hydrogen from thermo-chemical conversion of waste plastics, J. Anal. Appl. Pyrolysis. (2017) 0–1. https://doi.org/10.1016/j.jaap.2017.05.001.

[48] J.C. Acomb, C. Wu, P.T. Williams, Effect of growth temperature and feedstock:catalyst ratio on the production of carbon nanotubes and hydrogen from the pyrolysis of waste plastics, J. Anal. Appl. Pyrolysis. 113 (2015) 231–238. https://doi.org/10.1016/j.jaap.2015.01.012.

[49] Y. Zhang, P.T. Williams, Carbon nanotubes and hydrogen production from the pyrolysis catalysis or catalytic-steam reforming of waste tyres, J. Anal. Appl. Pyrolysis. 122 (2016) 490–501. https://doi.org/10.1016/j.jaap.2016.10.015.

[50] J. Liu, Z. Jiang, H. Yu, T. Tang, Catalytic pyrolysis of polypropylene to synthesize carbon nanotubes and hydrogen through a two-stage process, Polym. Degrad. Stab. 96 (2011) 1711–1719. https://doi.org/10.1016/j.polymdegradstab.2011.08.008.

[51] N. Mishra, G. Das, A. Ansaldo, A. Genovese, M. Malerba, M. Povia, D. Ricci, E. Di Fabrizio, E. Di Zitti, M. Sharon, M. Sharon, Pyrolysis of waste polypropylene for the synthesis of carbon nanotubes, J. Anal. Appl. Pyrolysis. 94 (2012) 91–98. https://doi.org/10.1016/j.jaap.2011.11.012.

[52] Y.S. Zhang, H.L. Zhu, D. Yao, P.T. Williams, C. Wu, D. Xu, Q. Hu, G. Manos, L. Yu, M. Zhao, P.R. Shearing, D.J.L. Brett, Thermo-chemical conversion of carbonaceous wastes for CNT and hydrogen production: A review, Sustain. Energy Fuels. 5 (2021) 4173–4208. https://doi.org/10.1039/d1se00619c.

[53] J. Bobek-Nagy, N. Gao, C. Quan, N. Miskolczi, D. Rippel-Pethő, K. Kovács, Catalytic co-pyrolysis of packaging plastic and wood waste to achieve H2 rich syngas, Int. J. Energy Res. 44 (2020) 10832–10845. https://doi.org/10.1002/er.5741.

[54] X. Gou, D. Zhao, C. Wu, Catalytic conversion of hard plastics to valuable carbon nanotubes, J. Anal. Appl. Pyrolysis. 145 (2020) 104748. https://doi.org/10.1016/j.jaap.2019.104748.

[55] T. Namioka, A. Saito, Y. Inoue, Y. Park, T. Min, S. Roh, K. Yoshikawa, Hydrogen-rich gas production from waste plastics by pyrolysis and low-temperature steam reforming over a ruthenium catalyst, Appl. Energy. 88 (2011) 2019–2026. https://doi.org/10.1016/j.apenergy.2010.12.053.

[56] C. Wu, P.T. Williams, Hydrogen from waste plastics by way of pyrolysis-gasification, Proc. Inst. Civ. Eng. Waste Resour. Manag. 167 (2014) 35–46. https://doi.org/10.1680/warm.13.00006.

[57] A. Erkiaga, G. Lopez, I. Barbarias, M. Artetxe, M. Amutio, J. Bilbao, M. Olazar, HDPE pyrolysis-steam reforming in a tandem spouted bed-fixed bed reactor for H2 production, J. Anal. Appl. Pyrolysis. 116 (2015) 34–41. https://doi.org/10.1016/j.jaap.2015.10.010.

[58] A. Ochoa, I. Barbarias, M. Artetxe, A.G. Gayubo, M. Olazar, J. Bilbao, P. Castano, Deactivation dynamics of a Ni supported catalyst during the steam reforming of volatiles from waste polyethylene pyrolysis, Appl. Catal. B Environ. 209 (2017) 554–565. https://doi.org/10.1016/j.apcatb.2017.02.015.

[59] I. Barbarias, G. Lopez, M. Artetxe, A. Arregi, L. Santamaria, J. Bilbao, M. Olazar, Pyrolysis and in-line catalytic steam reforming of polystyrene through a two-step reaction system, J. Anal. Appl. Pyrolysis. 122 (2016) 502–510. https://doi.org/10.1016/j.jaap.2016.10.006.

[60] M. Cortazar, N. Gao, C. Quan, M.A. Suarez, G. Lopez, S. Orozco, L. Santamaria, M. Amutio, M. Olazar, Analysis of hydrogen production potential from waste plastics by pyrolysis and in line oxidative steam reforming, Fuel Process. Technol. 225 (2022) 107044. https://doi.org/10.1016/j.fuproc.2021.107044.

[61] C. Garcia Lopez, A. Ni, J.C.H. Parrodi, B. Küppers, K. Raulf, T. Pretz, Characterization of Landfill Mining Material After Ballistic Separation To Evaluate Material and Energy Recovery Potential, Detritus. 08 (2019) 5–23. https://doi.org/10.31025/2611-4135/2019.13780.

[62] K. Jagodzińska, C. Garcia-Lopez, W. Yang, P.G. Jönsson, T. Pretz, K. Raulf, Characterisation of excavated landfill waste fractions to evaluate the energy recovery potential using Py-GC/MS and ICP techniques, Resour. Conserv. Recycl. 168 (2021). https://doi.org/10.1016/j.resconrec.2021.105446.

[63] J.M. Saad, P.T. Williams, Pyrolysis-catalytic dry (CO2) reforming of waste plastics for syngas production: Influence of process parameters, Fuel. 193 (2017) 7–14. https://doi.org/10.1016/j.fuel.2016.12.014.

[64] D. Yao, H. Li, Y. Dai, C.H. Wang, Impact of temperature on the activity of Fe-Ni catalysts for pyrolysis and decomposition processing of plastic waste, Chem. Eng. J. 408 (2021). https://doi.org/10.1016/j.cej.2020.127268.

[65] EN-ISO 18122:2015 - Solid biofuels — Determination of ash content, (2015).

[66] EN 15414-3:2011 - Solid recovered fuels - Determination of moisture content using the oven dry method - Part 3: Moisture in general analysis sample, (2011).

[67] 2011, EN 15407:2011 - Solid recovered fuels. Methods for the determination of carbon (C), hydrogen (H) and nitrogen (N) content, (n.d.).

[68] L. Dong, C. Wu, H. Ling, J. Shi, P.T. Williams, J. Huang, Promoting hydrogen production and minimizing catalyst deactivation from the pyrolysis-catalytic steam reforming of biomass on nanosized NiZnAlOx catalysts, Fuel. 188 (2017) 610–620. https://doi.org/10.1016/j.fuel.2016.10.072.

[69] M. Kruk, M. Jaroniec, Gas adsorption characterization of ordered organic-inorganic nanocomposite materials, Chem. Mater. 13 (2001) 3169–3183. https://doi.org/10.1021/cm0101069.

[70] D. Yao, H. Yang, Q. Hu, Y. Chen, H. Chen, P.T. Williams, Carbon nanotubes from post-consumer waste plastics: Investigations into catalyst metal and support material characteristics, Appl. Catal. B Environ. 280 (2021) 119413. https://doi.org/10.1016/j.apcatb.2020.119413.

[71] G. Gonçalves, M.K. Lenzi, O.A.A. Santos, L.M.M. Jorge, Preparation and characterization of nickel based catalysts on silica, alumina and titania obtained by sol-gel method, J. Non. Cryst. Solids. 352 (2006) 3697–3704. https://doi.org/10.1016/j.jnoncrysol.2006.02.120.

[72] J.M. Saad, M.A. Nahil, C. Wu, P.T. Williams, Influence of nickel-based catalysts on syngas production from carbon dioxide reforming of waste high density polyethylene, Fuel Process. Technol. 138 (2015) 156–163. https://doi.org/10.1016/j.fuproc.2015.05.020.

[73] J.Y. Park, Y.J. Lee, P.K. Khanna, K.W. Jun, J.W. Bae, Y.H. Kim, Alumina-supported iron oxide nanoparticles as Fischer-Tropsch catalysts: Effect of particle size of iron oxide, J. Mol. Catal. A Chem. 323 (2010) 84–90. https://doi.org/10.1016/j.molcata.2010.03.025.

[74] J.L. Pinilla, R. Utrilla, R.K. Karn, I. Suelves, M.J. Lázaro, R. Moliner, A.B. García, J.N. Rouzaud, High temperature iron-based catalysts for hydrogen and nanostructured carbon production by methane

decomposition, Int. J. Hydrogen Energy. 36 (2011) 7832–7843. https://doi.org/10.1016/j.ijhydene.2011.01.184.

[75] A. Griboval-Constant, A. Butel, V. V. Ordomsky, P.A. Chernavskii, A.Y. Khodakov, Cobalt and iron species in alumina supported bimetallic catalysts for Fischer-Tropsch reaction, Appl. Catal. A Gen. 481 (2014) 116–126. https://doi.org/10.1016/j.apcata.2014.04.047.

[76] L.R. Winter, E. Gomez, B. Yan, S. Yao, J.G. Chen, Tuning Ni-catalyzed CO2 hydrogenation selectivity via Ni-ceria support interactions and Ni-Fe bimetallic formation, Appl. Catal. B Environ. 224 (2018) 442–450. https://doi.org/10.1016/j.apcatb.2017.10.036.

[77] J. Huang, W. Liu, Y. Yang, B. Liu, High-Performance Ni-Fe Redox Catalysts for Selective CH4 to Syngas Conversion via Chemical Looping, ACS Catal. 8 (2018) 1748–1756. https://doi.org/10.1021/acscatal.7b03964.

[78] L. Wang, D. Li, M. Koike, S. Koso, Y. Nakagawa, Y. Xu, K. Tomishige, Catalytic performance and characterization of Ni-Fe catalysts for the steam reforming of tar from biomass pyrolysis to synthesis gas, Appl. Catal. A Gen. 392 (2011) 248–255. https://doi.org/10.1016/j.apcata.2010.11.013.

[79] J.M. Aguiar-Hualde, Y. Magnin, H. Amara, C. Bichara, Probing the role of carbon solubility in transition metal catalyzing single-walled carbon nanotubes growth, Carbon N. Y. 120 (2017) 226–232. https://doi.org/10.1016/j.carbon.2017.05.035.

[80] J. Sehested, Four challenges for nickel steam-reforming catalysts, Catal. Today. 111 (2006) 103–110. https://doi.org/10.1016/j.cattod.2005.10.002.

[81] H. Zhou, C. Wu, J.A. Onwudili, A. Meng, Y. Zhang, P.T. Williams, Polycyclic aromatic hydrocarbons (PAH) formation from the pyrolysis of different municipal solid waste fractions, Waste Manag. 36 (2015) 136–146. https://doi.org/10.1016/j.wasman.2014.09.014.

[82] S. Pathak, A.K. Sakhiya, A. Anand, K.K. Pant, P. Kaushal, A state-of-the-art review of various adsorption media employed for the removal of toxic Polycyclic aromatic hydrocarbons (PAHs): An approach towards a cleaner environment, J. Water Process Eng. 47 (2022) 102674. https://doi.org/10.1016/j.jwpe.2022.102674.

[83] W. Ye, X. Xu, M. Zhan, Q. Huang, X. Li, W. Jiao, Formation behavior of PAHs during pyrolysis of

waste tires, J. Hazard. Mater. 435 (2022) 1128997. https://doi.org/10.1016/j.jhazmat.2022.128997.

[84] P.H. Blanco, C. Wu, J.A. Onwudili, P.T. Williams, Characterization of Tar from the Pyrolysis/ Gasification of Refuse Derived Fuel: Influence of Process Parameters and Catalysis, Energy & Fuels. 26 (2012) 2107–2115. https://doi.org/10.1021/ef300031j.

[85] M.S. Seehra, V. Narang, U.K. Geddam, A.B. Stefaniak, Correlation between X-ray diffraction and Raman spectra of 16 commercial graphene–based materials and their resulting classification, Carbon N. Y. 111 (2017) 380–385. https://doi.org/10.1016/j.carbon.2016.10.010.

[86] M.A. Nahil, C. Wu, P.T. Williams, Influence of metal addition to Ni-based catalysts for the co-production of carbon nanotubes and hydrogen from the thermal processing of waste polypropylene, Fuel Process. Technol. 130 (2015) 46–53. https://doi.org/10.1016/j.fuproc.2014.09.022.

[87] S. Kumagai, J. Alvarez, P.H. Blanco, C. Wu, T. Yoshioka, M. Olazar, P.T. Williams, Novel Ni–Mg–Al–Ca catalyst for enhanced hydrogen production for the pyrolysis–gasification of a biomass/plastic mixture, J. Anal. Appl. Pyrolysis. 113 (2014) 15–21. https://doi.org/10.1016/j.jaap.2014.09.012.

[88] J.C. Acomb, C. Wu, P.T. Williams, Control of steam input to the pyrolysis-gasification of waste plastics for improved production of hydrogen or carbon nanotubes, Appl. Catal. B Environ. 147 (2014) 571–584. https://doi.org/10.1016/j.apcatb.2013.09.018.

[89] M. Artetxe, G. Lopez, G. Elordi, M. Amutio, J. Bilbao, M. Olazar, Production of Light Olefins from Polyethylene in a Two-Step Process: Pyrolysis in a Conical Spouted Bed and Downstream High-Temperature Thermal Cracking, Ind. Eng. Chem. Res. 51 (2012) 13915–13923. https://doi.org/10.1021/ie300178e.

[90] A. Veksha, K. Yin, J.G.S. Moo, W. Da Oh, A. Ahamed, W.Q. Chen, P. Weerachanchai, A. Giannis, G. Lisak, Processing of flexible plastic packaging waste into pyrolysis oil and multi-walled carbon nanotubes for electrocatalytic oxygen reduction, J. Hazard. Mater. 387 (2020) 121256. https://doi.org/10.1016/j.jhazmat.2019.121256.

[91] Y. Zhang, C. Wu, M.A. Nahil, P. Williams, Pyrolysis-Catalytic Steam Reforming/Gasification of Waste Tires for Production of Carbon Nanotubes and Hydrogen, Energy & Fuels. 29 (2015) 3328–3334. https://doi.org/10.1021/acs.energyfuels.5b00408.

[92] R.X. Yang, K.H. Chuang, M.Y. Wey, Effects of Nickel Species on Ni/Al2O3 Catalysts in Carbon Nanotube and Hydrogen Production by Waste Plastic Gasification: Bench- and Pilot-Scale Tests, Energy and Fuels. 29 (2015) 8178–8187. https://doi.org/10.1021/acs.energyfuels.5b01866.

[93] S.J. Park, K.D. Kim, Y.S. Park, K.S. Go, W. Kim, M.J. Kim, N.S. Nho, D.H. Lee, Effect of reduction conditions of Mo-Fe/MgO on the formation of carbon nanotube in catalytic methane decomposition, J. Ind. Eng. Chem. 109 (2022) 384–396. https://doi.org/10.1016/j.jiec.2022.02.023.

[94] P. Yan, K. Zhang, Y. Peng, Study of Fe2O3-Al2O3 catalyst reduction parameters and conditions for catalytic methane decomposition, Chem. Eng. Sci. 250 (2022) 117410. https://doi.org/10.1016/j.ces.2021.117410.

[95] J. Wang, B. Shen, M. Lan, D. Kang, C. Wu, Carbon nanotubes (CNTs) production from catalytic pyrolysis of waste plastics: The influence of catalyst and reaction pressure, Catal. Today. 351 (2020) 50–57. https://doi.org/10.1016/j.cattod.2019.01.058.

[96] C. Wu, M.A. Nahil, N. Miskolczi, J. Huang, P.T. Williams, Processing Real-World Waste Plastics by Pyrolysis-Reforming for Hydrogen and High-Value Carbon Nanotubes, Environ. Sci. Technol. 48 (2014) 819–826. https://doi.org//10.1021/es402488b.

[97] D. Xu, Y. Xiong, J. Ye, Y. Su, Q. Dong, S. Zhang, Performances of syngas production and deposited coke regulation during co-gasification of biomass and plastic wastes over Ni/γ-Al2O3 catalyst: Role of biomass to plastic ratio in feedstock, Chem. Eng. J. 392 (2020) 123728. https://doi.org/10.1016/j.cej.2019.123728.

[98] Y. Gomez-Rueda, I.N. Zaini, W. Yang, L. Helsen, Thermal tar cracking enhanced by cold plasma – A study of naphthalene as tar surrogate, Energy Convers. Manag. 208 (2020) 112540. https://doi.org/10.1016/j.enconman.2020.112540.

[99] A. Veksha, A. Giannis, G. Yuan, J. Tng, W.P. Chan, V.W.C. Chang, G. Lisak, T.T. Lim, Distribution and modeling of tar compounds produced during downdraft gasification of municipal solid waste, Renew. Energy. 136 (2019) 1294–1303. https://doi.org/10.1016/j.renene.2018.09.104.

Pyrolysis and in-line catalytic decomposition of excavated landfill waste to produce carbon nanotubes and hydrogen over Fe- and Ni-based catalysts – Investigation of the catalyst type and process temperature

Katarzyna Jagodzińska[1,*], Pär Göran Jönsson[1], Weihong Yang[1]

[1] KTH Royal Institute of Technology, Department of Material Sciences and Engineering, Brinellvägen 23, Stockholm, Sweden

[*] Corresponding author. E-mail address: kjag@kth.se (K. Jagodzińska).

Highlights

- It is a novel study on catalytic pyrolysis of excavated waste.
- Six Fe- and Ni- catalysts and three catalyst bed temperatures were considered.
- Catalysts were prepared using sol-gel and impregnation methods.
- The sol-gel catalysts outperformed the impregnation catalysts.
- The FeNi sol-gel catalyst yielded 9 mmol H_2 and 76 mg CNTs per g_{sample_daf}.

Declaration of interests

☒ The authors declare that they have no known competing financial interests or personal relationships that could have appeared to influence the work reported in this paper.

☐ The authors declare the following financial interests/personal relationships which may be considered as potential competing interests: